Rare Metal Materials and Engineering
Volume 52, Issue 3, March 2023
Available online at www.rmme.ac.cn

Science Press

Cite this article as: Xia Yuanjia, Zhao Fang, Liu Guoqing, et al. Multifunctional $Sn_{0.84}Sb_{0.08}Sm_{0.08}O_2$/TPU Composite Micro/Nano-Fiber Film for Infrared Stealth[J]. Rare Metal Materials and Engineering, 2023, 52(03): 852-859.

ARTICLE

Multifunctional $Sn_{0.84}Sb_{0.08}Sm_{0.08}O_2$/TPU Composite Micro/Nano-Fiber Film for Infrared Stealth

Xia Yuanjia[1], Zhao Fang[1], Liu Guoqing[1], Li Zhizun[1], Cheng Zhaogang[1], Zhang Yu[1], Li Ze[2]

[1] Shijiazhuang Campus, Army Engineering University of PLA, Shijiazhuang 050003, China; [2] Beijing Special Engineering Design and Research Institute, Beijing 100028, China

Abstract: The self-made hollow porous micro/nano-fiber structure $Sn_{0.84}Sb_{0.08}Sm_{0.08}O_2$ and thermoplastic polyurethane (TPU) were used as raw materials to prepare the $Sn_{0.84}Sb_{0.08}Sm_{0.08}O_2$/TPU (the addition content of $Sn_{0.84}Sb_{0.08}Sm_{0.08}O_2$ is 0wt%, 3wt%, 6wt%, and 9wt%) composite micro/nano-fiber films by electrostatic spinning method. Results show that the microstructures of composite films all present a fibrous 3D network structure. The tensile strength and elongation of the composite film are increased firstly and then decreased with increasing the addition content. When the addition amount is 6wt%, the tensile strength and elongation of the film are 2.68 MPa and 573%, which are 1.5 and 8.3 times higher than those of TPU film, respectively. The addition of $Sn_{0.84}Sb_{0.08}Sm_{0.08}O_2$ increases the thermal decomposition temperature and contact angle of the composite films to 303 °C and 120°, respectively. The infrared emissivity of the composite film is decreased with increasing the filler content. When the addition content is 9wt%, the infrared emissivity of the specimens at wavelength of 3–5 and 8–14 μm is 0.576 and 0.652, respectively. This composite film has good hydrophobicity, thermal stability, flexibility, and infrared stealth performance, providing experimental basis for the research of lightweight infrared stealth materials and showing certain application potential in the infrared stealth field.

Key words: infrared stealth; semiconductor; TPU; multifunctional; film

Infrared stealth materials have received extensive attention in the infrared camouflage[1], energy-saving windows[2], and heat shielding films[3] fields. According to the Stefan-Boltzmann law[4], $W=\sigma\varepsilon T^4$ (W is the amount of infrared radiation of the object; σ is the Boltzmann constant; ε is the emissivity of the object surface; T is the thermodynamic temperature of the object surface), when the material surface temperature is difficult to change, the lower the infrared emissivity of material, the better the infrared stealth performance. However, in the practical application, the material surface may be subjected to high temperature, high humidity, and severe impact. Thus, the infrared stealth materials with excellent thermal stability, hydrophobicity, and flexibility are highly required[5]. The infrared stealth materials with single function can hardly meet the practical application requirements, so the multifunctional infrared stealth materials show great potential.

Currently, the common infrared stealth materials mainly consist of inorganic low-emissivity fillers coupled with organic fillers. The combination of inorganic phase and organic phase can improve the comprehensive performance of the material, laying a certain foundation for the practical application[6]. Common fillers mainly include the metal and semiconductor. Although metal fillers have low infrared emissivity, their high density is detrimental to the stealth performance. The addition of semiconductor fillers can reduce the composite mass and improve the comprehensive properties through the morphology regulation and doping modification[7]. Common inorganic-organic composite materials with low emissivity are the coatings and thin films. The infrared stealth coatings have been widely researched, and the infrared stealth films have attracted even more attention due to their

Received date: June 23, 2022
Foundation item: Key Research and Development Program of Hebei Province (21351501D); Military Scientific Research Project (LJ20212C031165); Basic Frontier Science and Technology Innovation Project of Army Engineering University of PLA (KYSZJQZL2210)
Corresponding author: Liu Guoqing, Ph. D., Associate Professor, Shijiazhuang Campus, Army Engineering University of PLA, Shijiazhuang 050003, P. R. China, E-mail: 13081106809@163.com

good flexibility and permeability[8–10]. Fang et al[11] prepared ATO/PAN-$x$$VO_2$ (x=20wt%, 40wt%, 60wt%) composite fiber membrane by electrostatic spinning method, and found that the material has good infrared stealth performance, thermal adaptability, and mechanical properties. Fang et al[12] prepared ZnO(Al, La)/PAN fiber film by electrostatic spinning method, and reported that its infrared emissivity at wavelength of 8–14 μm is 0.793. Jeong et al[13] developed the wearable ATO/PU composite fiber fabric and found that the fabric has good mechanical properties and hydrophobicity, showing great potential in cloth manufacture. Thermopolymer polyurethane (TPU) has excellent flexibility, hydrolysis resistance, and abrasion resistance[14–15], which is widely used in sensors[16], lithium batteries[17], and medical materials[18] due to its high quality and low cost. TPU is a fine matrix material for functional fillers to increase and optimize the composite functionality[15].

The electrostatic spinning method was combined with heat treatment to prepare the $Sn_{0.84}Sm_{0.08}Sb_{0.08}O_2$ micro/nano-fiber material with hollow porous structure, and the prepared material had low infrared emissivity of 0.558 and 0.672 at wavelength of 3–5 and 8–14 μm, respectively, showing great potential as a functional filler with low infrared emissivity. Therefore, in this research, the $Sn_{0.84}Sm_{0.08}Sb_{0.08}O_2$ micro/nano-fiber material with hollow porous structure was used as filler, TPU was used as binder, and the $Sn_{0.84}Sm_{0.08}Sb_{0.08}O_2$/TPU composite micro/nano-fiber films with $Sn_{0.84}Sm_{0.08}Sb_{0.08}O_2$ addition of 0wt%, 3wt%, 6wt%, and 9wt% were prepared by electrostatic spinning method. The thermal stability, mechanical properties, hydrophobicity, and infrared stealth properties of composite films were investigated. This research provided a certain experimental basis for the development of high-temperature-resistant, lightweight, and easily-prepared multifunctional infrared stealth film.

1 Experiment

$SnCl_2·2H_2O$, $Sm(NO_3)_3·6H_2O$, and $SbCl_3$ were used as raw materials and dissolved in anhydrous ethanol according to the stoichiometrical ratio of $Sn_{0.84}Sm_{0.08}Sb_{0.08}O_2$. The solution was mixed with polyvinyl pyrrolidone (PVP) + N, N-dimethyl-formamide (DMF) solution in the mass ratio of 1:2 and stirred for 12 h to prepare the shell solution. PVP was dissolved in DMF+anhydrous ethanol solution in the mass ratio of 1:2 and stirred for 12 h to prepare the core solution. The shell solution was put into the outer container of the coaxial electrostatic spinning device, and the core solution was put into the inner container of the coaxial electrostatic spinning device. The coaxial electrostatic spinning was conducted at voltage of 18 kV with the outer diameter of coaxial stainless steel needle of 1.4 mm, inner diameter of coaxial stainless steel needle of 0.7 mm, flow rate of shell/core solution of 0.05 mL/h, distance between needle and receiver of 20 cm, and the receiving speed of 140 r/min. The precursor micro/nano-fibers were firstly dried in a vacuum drying oven at 100 °C for 12 h, then placed in an intelligent temperature control box of resistance furnace, heated to 600 °C at heating rate of 3 °C/min, calcined for 2 h, and finally cooled to room temperature in the furnace.

The analytical pure TPU and the hollow porous $Sn_{0.84}Sm_{0.08}Sb_{0.08}O_2$ micro/nano-fibers were used as raw materials. The addition content of $Sn_{0.84}Sb_{0.08}Sm_{0.08}O_2$ was 0wt%, 3wt%, 6wt%, and 9wt%. $Sn_{0.84}Sb_{0.08}Sm_{0.08}O_2$ was added according to the stoichiometrical ratio and dissolved in a mixed solution of DMF+tetrahydrofuran (THF) with the mass ratio of DMF:THF =3:2. Firstly, the solution was ultrasonically dispersed for 30 min and then magnetically stirred for 6 h to prepare the spinning precursor solution. The precursor solution was transferred into a syringe with stainless steel needle for electrostatic spinning. The spinning was conducted at room temperature under voltage of 15 kV, spinning needle diameter of 0.75 mm, distance between needle and receiver of 20 cm, solution propulsion speed of 0.2 mL/h, and receiving speed of 140 r/min. The spun films were dried in a vacuum drying oven at 50 °C for 6 h. The schematic diagram of preparation process is shown in Fig.1.

Thermogravimetric analysis (TGA) was performed by differential thermogravimetric analyzer (SDT-Q600, TA, USA). The specimen phases were analyzed by polycrystalline X-ray diffractometer (XRD, XD6, Purkinje, China). The infrared spectrum analysis of the specimens was conducted by Fourier transform infrared spectrometer (380, Nicolet, USA). The specimen morphologies were characterized by field emission scanning electron microscope (SEM, SU-8010, HITACHI, Japan). The contact angle tests were conducted by the contact angle tester (OCA40, Dataphysics, Germany). The infrared emissivity of the specimens was tested by the IR-2 dual-band infrared emissivity tester (FT-IR, Chengbo, China). The infrared thermal images of specimens were taken by infrared thermal imager (120S, UTi, China). The mechanical properties of the specimens were tested by universal testing machine (5982, INSTRON, USA).

2 Results and Discussion

2.1 XRD analysis

Fig. 2 shows XRD patterns of specimens with different $Sn_{0.84}Sm_{0.08}Sb_{0.08}O_2$ addition contents. It can be seen that the specimens with different $Sn_{0.84}Sm_{0.08}Sb_{0.08}O_2$ addition contents all have broad dispersion peaks at around 2θ=20°, indicating that TPU is an amorphous substance. Besides, with increasing

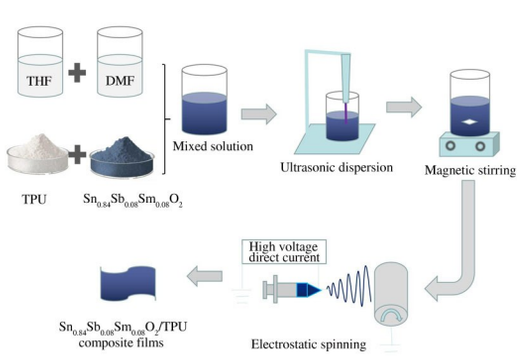

Fig.1 Schematic diagram of preparation process

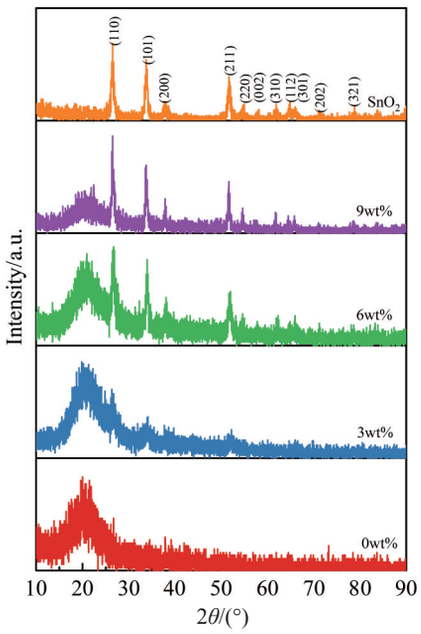

Fig.2 XRD patterns of SnO_2 and different $Sn_{0.84}Sb_{0.08}Sm_{0.08}O_2$/TPU composite micro/nano-fiber films

the addition content of $Sn_{0.84}Sm_{0.08}Sb_{0.08}O_2$, the diffraction peaks of each specimen at (110), (101), (200), (211), and (220) crystal planes become obvious and sharp. The intensity of main diffraction peaks is arranged from the strongest to the weakest as (110)>(101)>(211)>(200), which is consistent with JCPDS41-1445 reference, indicating that the doped $Sn_{0.84}Sm_{0.08}Sb_{0.08}O_2$ is rutile SnO_2.

2.2 FT-IR analysis

In order to further clarify the phase structure of the specimens, FT-IR analysis was conducted on the 6wt% $Sn_{0.84}Sb_{0.08}Sm_{0.08}O_2$/TPU composite micro/nano-fiber film, as shown in Fig.3. It can be seen that the absorption peaks appear

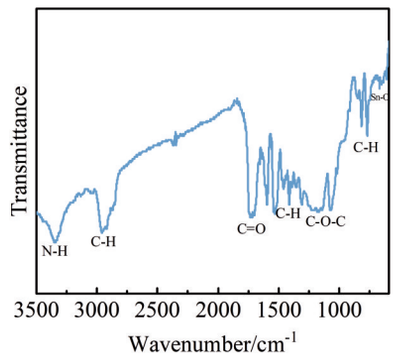

Fig.3 FT-IR spectrum of 6wt% $Sn_{0.84}Sb_{0.08}Sm_{0.08}O_2$/TPU composite micro/nano-fiber film

at 2943, 1411, and 713 cm^{-1}, which are caused by the tensile vibration of C-H in TPU[19]. The absorption peaks at 3350 cm^{-1} can be attributed to the N-H groups in TPU[20], and those at 1717 and 1100–1280 cm^{-1} are related to the C=O and C-O-C groups, respectively[21]. Besides, the absorption peak of SnO_2 can also be observed at around 610 cm^{-1} [22], which belongs to the E_uTO vibration mode[23]. This is consistent with the XRD analysis results.

2.3 SEM analysis

Fig. 4 shows SEM morphologies and fiber diameter distributions of $Sn_{0.84}Sb_{0.08}Sm_{0.08}O_2$/TPU composite micro/nano-fiber films. It can be seen that all specimens are fibrous, and the fibers are interlaced with each other, forming a three-dimensional network structure. The average fiber diameter of all specimens is 300 – 400 nm, and the fiber diameter is increased gradually with increasing the filler content. When the $Sn_{0.84}Sb_{0.08}Sm_{0.08}O_2$ addition is 0wt%, the fiber surface is smooth and the fiber has good continuity. When the $Sn_{0.84}Sb_{0.08}Sm_{0.08}O_2$ addition increases to 3wt%, the fiber diameter is increased and its distribution becomes dispersed. When the $Sn_{0.84}Sb_{0.08}Sm_{0.08}O_2$ addition further increases to

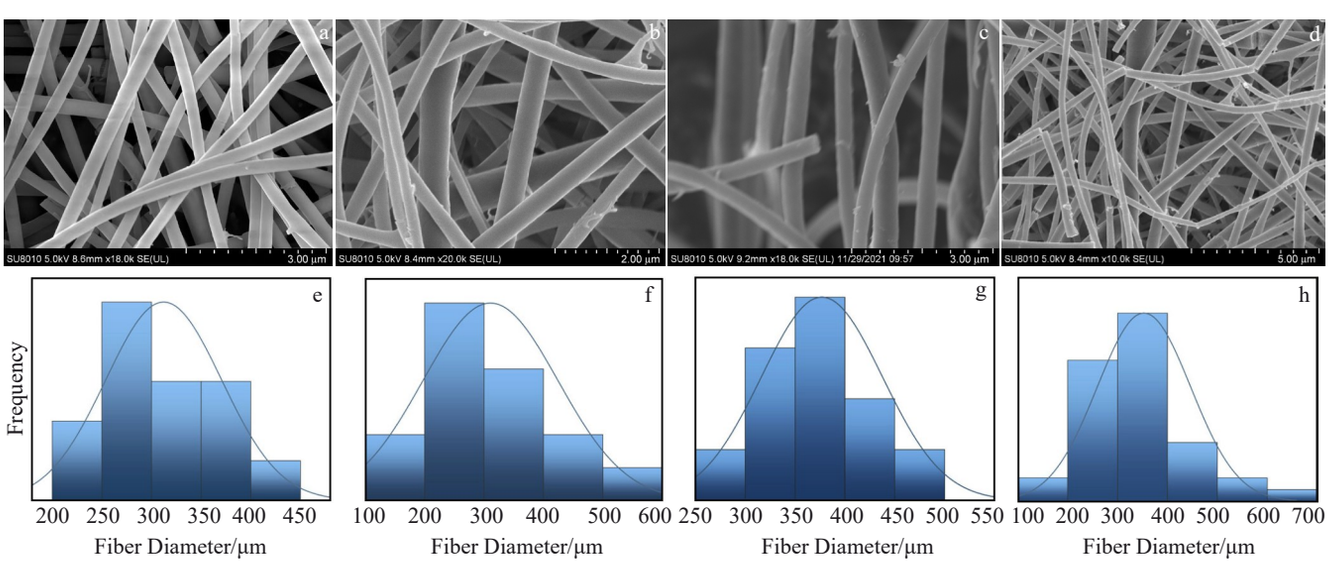

Fig.4 SEM morphologies (a–d) and fiber diameter distributions (e–h) of different $Sn_{0.84}Sb_{0.08}Sm_{0.08}O_2$/TPU composite micro/nano-fiber films: (a, e) 0wt%, (b, f) 3wt%, (c, g) 6wt%, and (d, h) 9wt%

6wt% , although a small number of specimen fibers are broken, they are locally oriented and arranged and the fiber diameter distribution is relatively uniform. When the $Sn_{0.84}Sb_{0.08}Sm_{0.08}O_2$ addition is 9wt% , the fiber continuity decreases, some fibers are broken, and the fiber diameter distribution is dispersed. The difference in fiber diameter distribution and fiber continuity may be related to the effect of different additive contents on the properties of spinning solution.

2.4 TGA

Fig. 5 shows TGA curves of different $Sn_{0.84}Sb_{0.08}Sm_{0.08}O_2$/TPU composite micro/nano-fiber films. It can be seen that the thermal decomposition of $Sn_{0.84}Sb_{0.08}Sm_{0.08}O_2$/TPU composite micro/nano-fiber film can be divided into four stages. The first stage is from room temperature to 303 °C. At this stage, the TGA curves are basically horizontal, and the mass loss is slight, indicating that the specimens have a certain thermal stability from room temperature to 303 °C. It can also be observed that the thermal decomposition temperature of fiber film is increased from 274 °C to 303 °C after $Sn_{0.84}Sb_{0.08}Sm_{0.08}O_2$ is added into the TPU film, indicating that the introduction of $Sn_{0.84}Sb_{0.08}Sm_{0.08}O_2$ can improve the thermal stability and thermal decomposition temperature of TPU. The second stage is 303–380 °C, where obvious mass loss occurs. The mass loss of all specimens is about 75%, which may be caused by the decomposition of TPU hard segment, i.e., the break of polyurethane bonds, thus generating diisocyanate and diol and releasing carbon dioxide[24]. The third stage is 380–480 °C, where the mass loss rate slows down. This may be caused by the decomposition of TPU soft segment, i.e., the decomposition of polyols[25]. The fourth stage is 480–700 °C. In this stage, the TGA curves are stable and horizontal, and there are only a small amount of residue and $Sn_{0.84}Sb_{0.08}Sm_{0.08}O_2$ in the thermal decomposition products. The mass of calcined residue is increased with increasing the $Sn_{0.84}Sb_{0.08}Sm_{0.08}O_2$ filler content, and the residual proportion is basically consistent with the addition proportion.

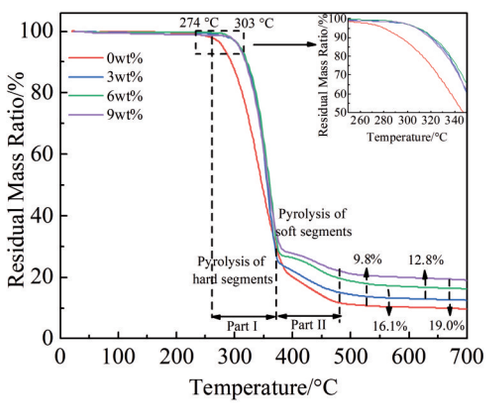

Fig.5 TGA curves of different $Sn_{0.84}Sb_{0.08}Sm_{0.08}O_2$/TPU composite micro/nano-fiber films

2.5 Hydrophobicity analysis

Fig. 6a shows the contact angles of different $Sn_{0.84}Sb_{0.08}Sm_{0.08}O_2$/TPU composite micro/nano-fiber films. It can be seen that the addition of $Sn_{0.84}Sm_{0.08}Sb_{0.08}O_2$ micro/nano-fiber filler into the TPU film has a significant effect on the contact angle of films. When the $Sn_{0.84}Sm_{0.08}Sb_{0.08}O_2$ addition increases to 3wt%, the contact angle of TPU film increases from 106° to 114° . When the $Sn_{0.84}Sm_{0.08}Sb_{0.08}O_2$ addition is 9wt% , the contact angle of composite film is about 120°. Although the contact angle of composite films is different from that of the super hydrophobic material (150°), it is still much higher than the contact angle required in hydrophobic standard (90°). The appearances of contact angles of different composite films are

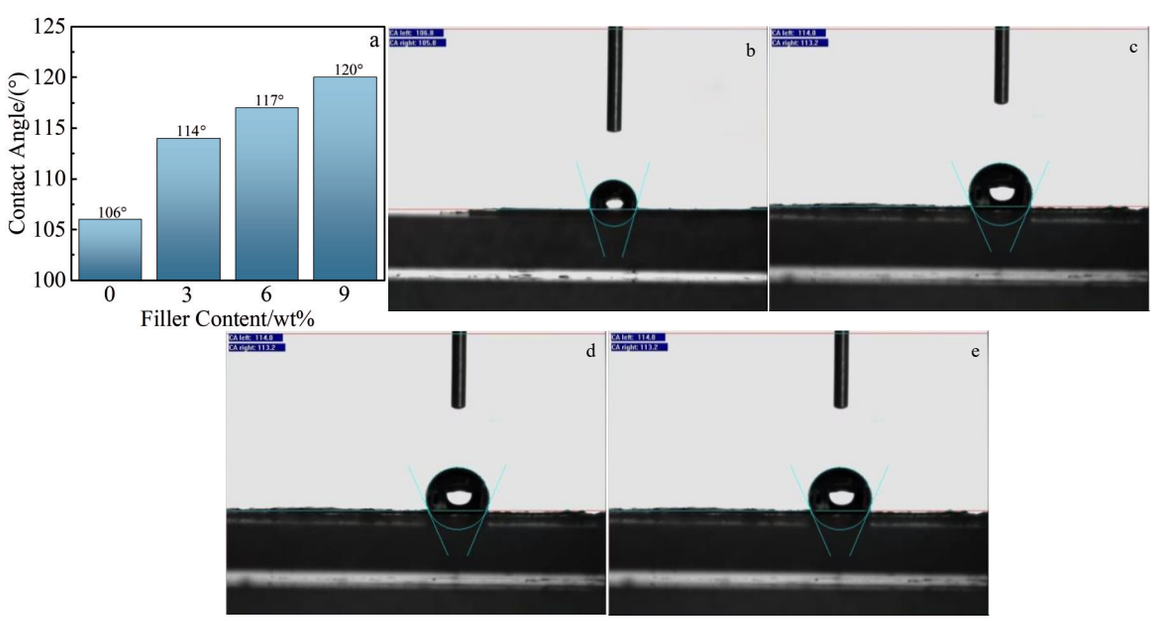

Fig.6 Contact angle results (a) and appearances of contact angles (b–e) of different $Sn_{0.84}Sb_{0.08}Sm_{0.08}O_2$/TPU composite micro/nano-fiber films: (b) 0wt%, (c) 3wt%, (d) 6wt%, and (e) 9wt%

shown in Fig. 6b – 6e. The main reason for the increase in contact angle is that the $Sn_{0.84}Sb_{0.08}Sm_{0.08}O_2$ micro/nano-fibers have good hydrophobic performance, and the hydrophobic micro/nano-fibers are evenly distributed in TPU matrix, which increases the vapor/liquid interface between water droplets and the film to a certain extent, reduces the surface energy of composite film, and enhances the hydrophobic performance[26].

2.6 Mechanical properties

Fig. 7a – 7c show the stress-strain curves, tensile strength, and elongation of different $Sn_{0.84}Sb_{0.08}Sm_{0.08}O_2$/TPU composite micro/nano-fiber films. It can be seen that when the $Sn_{0.84}Sb_{0.08}Sm_{0.08}O_2$ addition increases from 0wt% to 3wt%, the tensile strength increases from 1.82 MPa to 4.95 MPa. The tensile strength of 3wt% $Sn_{0.84}Sb_{0.08}Sm_{0.08}O_2$/TPU composite micro/nano-fiber film is 2.72 times higher than that without fillers. The elongation is increased from 69% to 161% with increasing the $Sn_{0.84}Sb_{0.08}Sm_{0.08}O_2$ addition from 0wt% to 3wt% . The elongation of 3wt% $Sn_{0.84}Sb_{0.08}Sm_{0.08}O_2$/TPU composite micro/nano-fiber film is 2.33 times higher than that without fillers. The appearances of 3wt% $Sn_{0.84}Sb_{0.08}Sm_{0.08}O_2$/TPU composite micro/nano-fiber film before and after stretching are shown in Fig. 7d_1 and 7d_2, respectively. When the $Sn_{0.84}Sb_{0.08}Sm_{0.08}O_2$ addition further increases to 6wt%, the mechanical properties of the film are further improved. The tensile strength and elongation are 2.68 MPa and 573%, which are 1.5 and 8.3 times higher than those without fillers. The appearances of 6wt% $Sn_{0.84}Sb_{0.08}Sm_{0.08}O_2$/TPU composite micro/nano-fiber film before and after stretching are shown in Fig. 7e_1 and 7e_2, respectively. When the $Sn_{0.84}Sb_{0.08}Sm_{0.08}O_2$ addition is 9wt%, the tensile strength is reduced to 1.21 MPa and the elongation is 230%, indicating that the tensile strength is decreased but the elongation is increased with excess filler addition, compared with those without filler. In general, the tensile strength and elongation of the specimens are increased firstly and then decreased with increasing the filler content. This is because in the $Sn_{0.84}Sb_{0.08}Sm_{0.08}O_2$/TPU composite fiber films, a small amount of $Sn_{0.84}Sb_{0.08}Sm_{0.08}O_2$ fills the defects of TPU matrix. The fibers can maintain the good continuity and smoothness with appropriate addition amount, as shown in Fig.4b, so the mechanical properties of composite film can be greatly improved. With excess addition of filler, the continuity of fibers is decreased, some fibers begin to break, and the surface smoothness is also decreased to a certain extent, as shown in Fig.4d, which results in the reduction of mechanical properties. When the filler content is 6wt% , the composite micro/nano-fiber film has the highest elongation, which may be related to the local orientation of fibers and the uniform fiber diameter distribution. Compared with disordered fibers, the oriented fibers with uniform diameters have stronger tensile strength and larger fracture strain, which can effectively improve the strength and plasticity of the specimens[27].

2.7 Infrared emissivity and thermal imaging analysis

Fig. 8 and Fig. 9 show infrared emissivity, morphologies, and infrared thermal images of $Sn_{0.84}Sb_{0.08}Sm_{0.08}O_2$/TPU composite micro/nano-fiber films. Fig. 8a shows the infrared emissivity of different $Sn_{0.84}Sb_{0.08}Sm_{0.08}O_2$/TPU composite micro/nano-fiber films. It can be seen that with increasing the $Sn_{0.84}Sb_{0.08}Sm_{0.08}O_2$ addition, the infrared emissivity of the

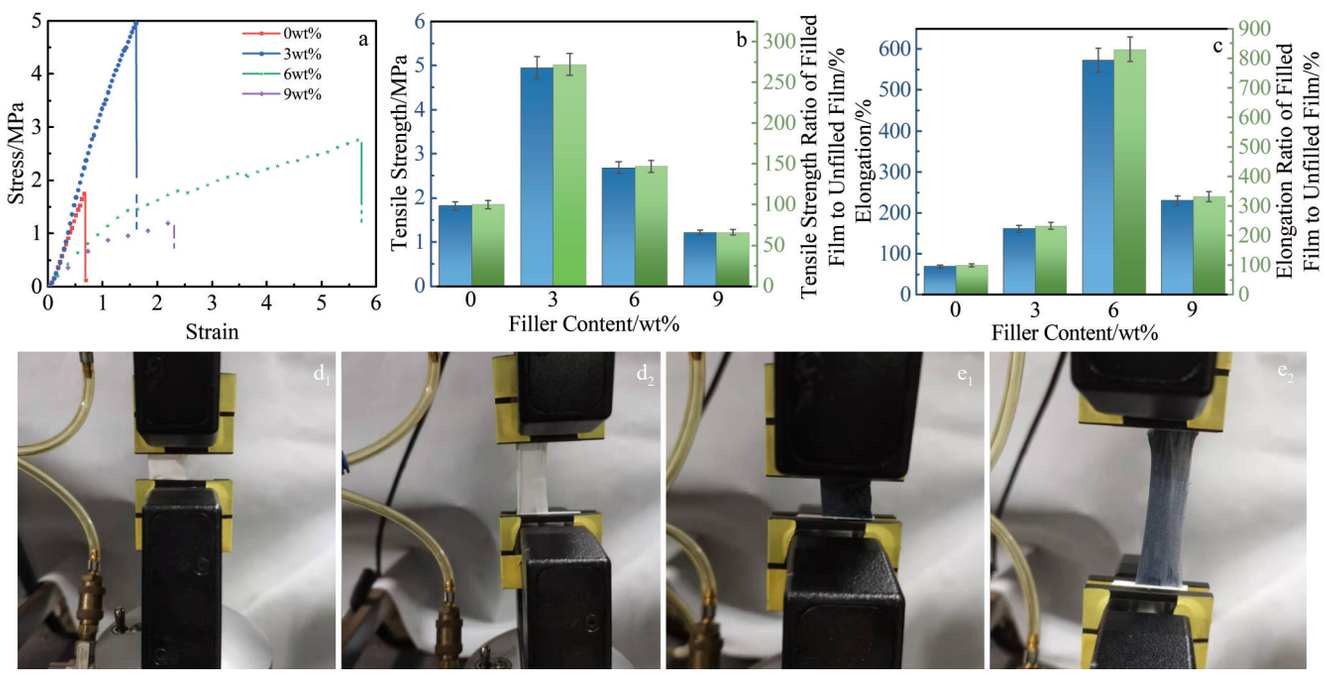

Fig.7 Stress-strain curves (a), tensile strength (b), and elongation (c) of different $Sn_{0.84}Sb_{0.08}Sm_{0.08}O_2$/TPU composite micro/nano-fiber films; appearances of 3wt% (d_1, d_2) and 6wt% (e_1, e_2) $Sn_{0.84}Sb_{0.08}Sm_{0.08}O_2$/TPU composite micro/nano-fiber films before (d_1, e_1) and after (d_2, e_2) stretching

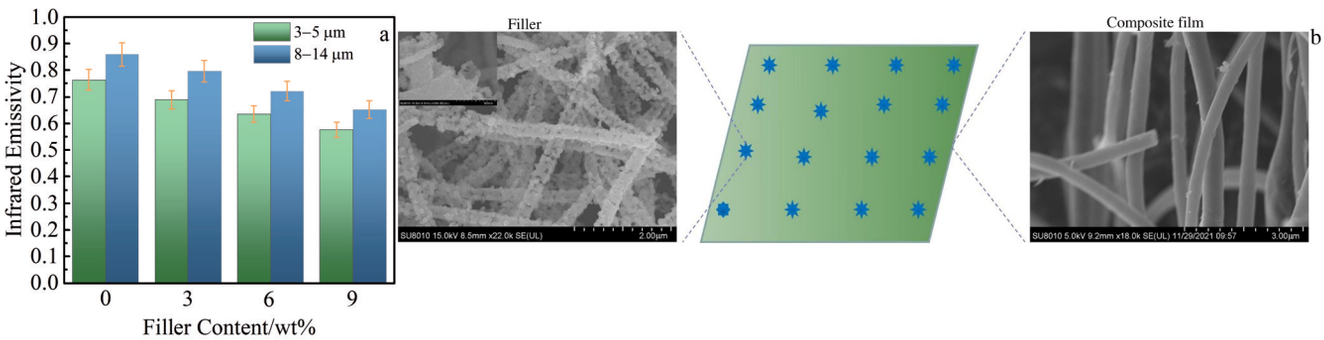

Fig.8 Infrared emissivity of different $Sn_{0.84}Sb_{0.08}Sm_{0.08}O_2$/TPU composite micro/nano-fiber films (a); SEM morphologies and schematic diagram of composite micro/nano-fiber film and filler (b)

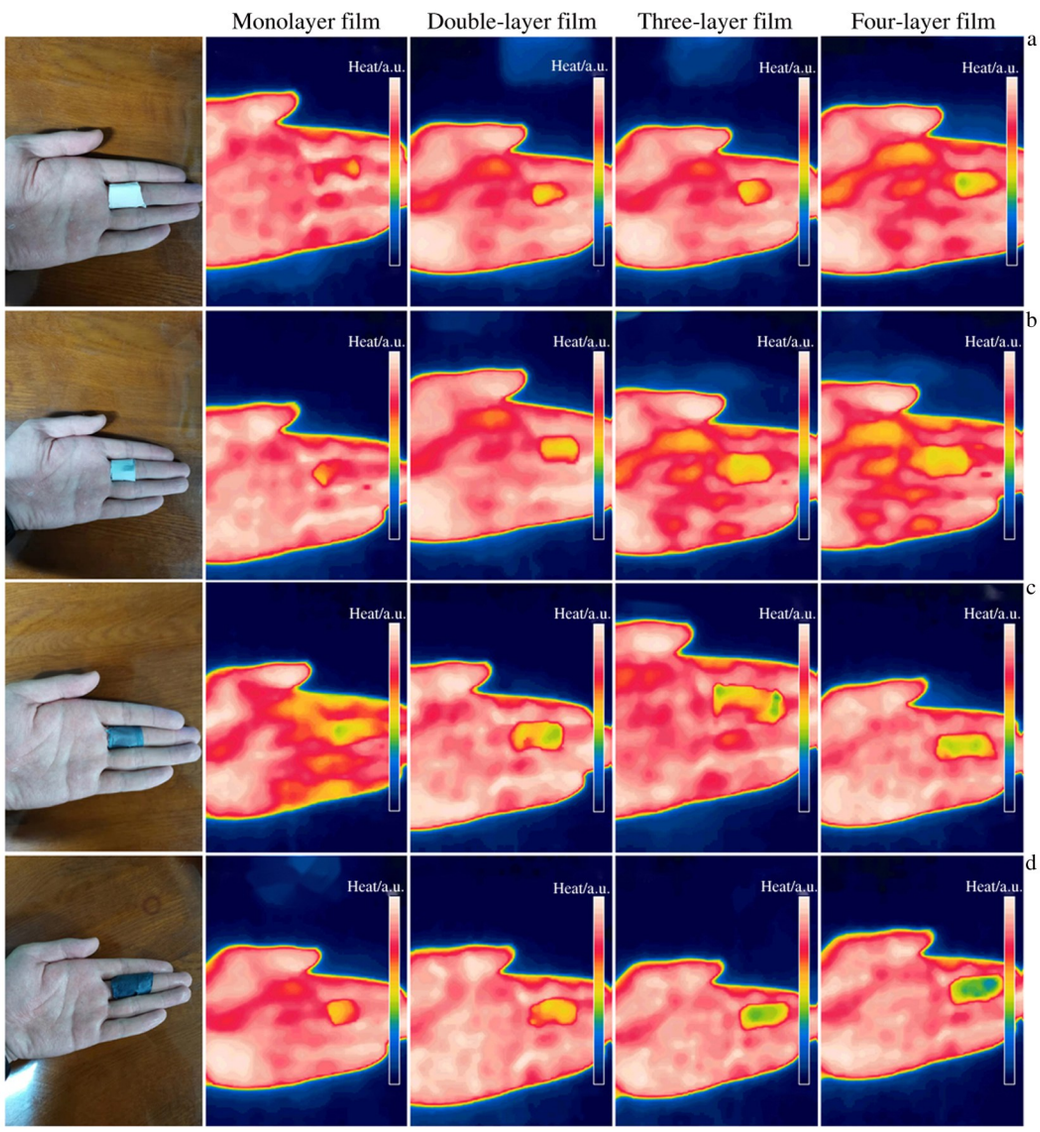

Fig.9 Infrared thermal imaging images of 0wt% (a), 3wt% (b), 6wt% (c), and 9wt% (d) $Sn_{0.84}Sm_{0.08}Sb_{0.08}O_2$/TPU composite micro/nano-fiber films under different numbers of membrane layers

specimens at wavelength of 3–5 and 8–14 μm is decreased. When the $Sn_{0.84}Sb_{0.08}Sm_{0.08}O_2$ addition is 9wt%, the infrared emissivity of specimens at wavelength of 3–5 and 8–14 μm is 0.576 and 0.652, respectively. The reasons for the decrease in infrared emissivity are as follows. First of all, the microstructure of composite micro/nano-fiber film presents a

fibrous three-dimensional network, and the $Sn_{0.84}Sm_{0.08}Sb_{0.08}O_2$ filler with low emissivity is distributed among the fibers, thus forming a conductive network. Secondly, the $Sn_{0.84}Sm_{0.08}Sb_{0.08}O_2$ filler is composed of porous hollow fiber, which can effectively reduce the infrared emissivity. This is the main mechanism of infrared emissivity loss of composite film. The dual infrared emissivity regulation mechanism can also effectively reduce the infrared emissivity of specimens. SEM images of composite micro/nano-fiber films and fillers are shown in Fig.8b.

In order to further characterize the infrared stealth performance of $Sn_{0.84}Sm_{0.08}Sb_{0.08}O_2$/TPU composite micro/nano-fiber films, the infrared thermal imaging images of different specimens under different numbers of membrane layers were recorded, as shown in Fig.9. It can be seen that the infrared stealth performance is improved with increasing the $Sn_{0.84}Sm_{0.08}Sb_{0.08}O_2$ filler content. In addition, with increasing the number of layers of the composite film, the infrared stealth performance is also enhanced. When the filler content is 6wt% and 9wt% , the specimen has good infrared stealth performance. The thickness of four layers of composite fiber film is 0.18–0.19 mm, which is still an ultra-thin thickness, thus showing good infrared stealth performance with a broad application prospect.

3 Conclusions

1) The microstructure of the $Sn_{0.84}Sm_{0.08}Sb_{0.08}O_2$/thermoplastic polyurethane (TPU) composite micro/nano-fiber films is a fibrous three-dimensional network, and the fiber continuity is decreased with increasing the filler content.

2) The addition of $Sn_{0.84}Sm_{0.08}Sb_{0.08}O_2$ filler increases the thermal decomposition temperature of TPU film from 274 °C to 303 ° C, decreases the surface energy of TPU film, and increases the contact angle to 120° , indicating that the composite fiber film has good thermal stability and hydrophobicity.

3) Appropriate addition of $Sn_{0.84}Sm_{0.08}Sb_{0.08}O_2$ filler can fill the defects in TPU film and enhance the mechanical properties. When the filler content increases from 0wt% to 3wt% , the tensile strength of the composite film increases from 1.82 MPa to 4.95 MPa, and the elongation increases from 69% to 161%. When the filler content is 6wt% , the tensile strength and elongation of the composite film is 2.68 MPa and 573%, which are 1.5 and 8.3 times higher than those without filler addition, respectively.

4) The addition of $Sn_{0.84}Sm_{0.08}Sb_{0.08}O_2$ filler improves the infrared stealth performance of composite film. When the addition amount is 9wt% , the infrared emissivity of the composite film at wavelength of 3–5 and 8–14 μm is 0.576 and 0.652, respectively. With increasing the filler content and the number of film layers, the infrared stealth performance of the composite micro/nano-fiber film is enhanced. This research provides a certain experimental basis for the development of high-temperature-resistant, lightweight, and easily-prepared multifunctional infrared stealth film.

References

1 Chai X, Zhu D M, Liu Y *et al. Composites Science and Technology*[J], 2021, 216: 109 038

2 Aburas M, Soebarto V, Williamson T *et al. Applied Energy*[J], 2019, 255: 113 522

3 Lyu J, Liu Z W, Wu X H *et al. ACS Nano*[J], 2019, 13(2): 2236

4 Sheehan D P. *Entropy*[J], 2012, 14(10): 1915

5 Feng Lili, Liu Yiman, Yao Lin *et al. Progress in Chemistry*[J], 2021, 33(6): 1044 (in Chinese)

6 Shen Yulian, Li Chunhai, Guo Shaoyun *et al. Infrared Technology*[J], 2021, 43(4): 312 (in Chinese)

7 Liu Xiaoming, Ren Zhiyu, Chen Luping *et al. Journal of Materials Engineering*[J], 2020, 48(6): 1 (in Chinese)

8 Chung J, Lee S. *Fibers and Polymers*[J], 2014, 15(6): 1153

9 Mao X, Bai Y, Yu J Y *et al. Dalton Transactions*[J], 2016, 45(15): 6660

10 Fang K Y, Zhao Y C, Fang F. *Journal of Alloys and Compounds*[J], 2021, 855(1): 157 418

11 Fang K Y, Wang Y J, Zhao Y C *et al. Composites Science and Technology*[J], 2021, 201: 108 483

12 Fang S J, Wang W, Yu X L *et al. Materials Letters*[J], 2015, 143: 120

13 Jeong S M, Ahn J, Choi Y K *et al. NPG Asia Materials*[J], 2020, 12(1): 32

14 Cao N N, Zheng Y Y, Liu Y L *et al. Acta Materiae Composite Sinica*[J], 2016, 33(7): 1371

15 Zhang J, Li X, Guo J *et al. Materials Advances*[J], 2022, 3(3): 1518

16 Li Y, Wang S, Xiao Z C *et al. Journal of Materials Chemistry C*[J], 2020, 8(12): 4040

17 Cai M, Zhu J W, Yang C C *et al. Polymers*[J], 2019, 11(1): 185

18 Grenier S, Sandig M, Mequanint K. *Journal of Biomedical Materials Research Part A*[J], 2007, 82(4): 802

19 Fang H, Zhang L J, Chen A L *et al. Polymers*[J], 2022, 14(8): 1530

20 Zhou J, Cai Q, Liu X *et al. Nanoscale Research Letters*[J], 2018, 13(1): 384

21 Jiang Y H, Li F, Mei Y F *et al. Journal of Materials Science*[J], 2021, 56(3): 2474

22 Al-Saadi T M, Hussein B H, Hasan A B *et al. Energy Procedia*[J], 2019, 157: 457

23 Yang P, Lieber C M. *Science*[J], 1996, 273(5283): 1836

24 Chattopadhyay D K, Webster D C. *Progress in Polymer Science*[J], 2009, 34(10): 1068

25 Herrera M, Matuschek G, Kettrup A. *Polymer Degradation and Stability*[J], 2002, 78(2): 323

26 Wang L F, Yang S Y, Wang J *et al*. *Materials Letters*[J], 2011, 65(5): 869

27 Lee H, Watanabe K, Kim M *et al*. *Scientific Reports*[J], 2016, 6: 37 590

可用于红外隐身的多功能$Sn_{0.84}Sb_{0.08}Sm_{0.08}O_2$/TPU复合微纳米纤维薄膜

夏元佳[1]，赵　芳[1]，刘国庆[1]，李志尊[1]，程兆刚[1]，张　宇[1]，李　泽[2]

(1. 陆军工程大学石家庄校区，河北 石家庄 050003)

(2. 北京特种工程设计研究院，北京 100028)

摘　要：以自制的中空多孔微纳纤维结构$Sn_{0.84}Sb_{0.08}Sm_{0.08}O_2$和热塑性聚氨酯（TPU）为原料，利用静电纺丝法制备$Sn_{0.84}Sb_{0.08}Sm_{0.08}O_2$/TPU（$Sn_{0.84}Sb_{0.08}Sm_{0.08}O_2$添加质量分数为0%、3%、6%和9%）复合微纳米纤维薄膜。结果表明：复合薄膜的微观形貌均呈现纤维状三维网络结构；复合薄膜的抗拉伸强度和伸长率随着添加量的增加均呈现先增强后减弱的趋势，当添加量为6%时，薄膜的抗拉伸强度为2.68 MPa，伸长率为573%，是TPU薄膜的1.5和8.3倍。$Sn_{0.84}Sb_{0.08}Sm_{0.08}O_2$的添加将复合薄膜的热分解温度和接触角分别提升至303 ℃和120°。复合薄膜的红外发射率随$Sn_{0.84}Sb_{0.08}Sm_{0.08}O_2$添加量的增加而逐渐减小，当添加量为9%时，样品在3~5和8~14 μm波长区间的红外发射率分别为0.576和0.652。本研究制备的复合薄膜具有良好的疏水性、热稳定性、柔韧性和红外隐身性能，为轻质红外隐身材料的研究提供了实验依据，在红外隐身领域具有一定的应用前景。

关键词：红外隐身；半导体；TPU；多功能化；薄膜

作者简介：夏元佳，男，1998年生，硕士生，陆军工程大学石家庄校区，河北 石家庄 050003，E-mail：1220563265@qq.com